Real-Time Frequency Response Estimation Using Joined-Wing SensorCraft Aeroelastic Wind-Tunnel Data

Jared Grauer*, Jennifer Heeg†, and Eugene Morelli‡
NASA Langley Research Center, Hampton, Virginia, 23666

A new method is presented for estimating frequency responses and their uncertainties from wind-tunnel data in real time. The method uses orthogonal phase-optimized multisine excitation inputs and a recursive Fourier transform with a least-squares estimator. The method was first demonstrated with an F-16 nonlinear flight simulation and results showed that accurate short period frequency responses were obtained within 10 seconds. The method was then applied to wind-tunnel data from a previous aeroelastic test of the Joined-Wing SensorCraft. Frequency responses describing bending strains from simultaneous control surface excitations were estimated in a time-efficient manner.

Nomenclature

Symbols

a, b	input and output amplitudes
$G(j\omega)$	frequency response
j	imaginary number $\sqrt{-1}$
K	set of excitation frequency indices
N	number of data samples
n_f	number of Fourier transform samples
n_ω	total number of excitation frequencies
$\Re$	real part
T	record length [s]
t	time [s]
u	input
$\mathbf{X}$	regressor matrix
y	output
Δ	perturbation
δ	control surface deflection [deg]
ϵ	bending strain
$\boldsymbol{\theta}$	unknown parameters
$\boldsymbol{\Sigma}$	covariance matrix
σ^2	variance
ϕ, ψ	input and output phase angles [rad]
ω	frequency [rad/s]
$\|.\|$	magnitude
$\angle$	phase angle

Superscripts

^{T}	transpose
$^{-1}$	inverse
†	complex conjugate transpose
$\dot{}$	time derivative
$\hat{}$	estimated value
$\tilde{}$	Fourier transform

Subscripts

$_{AW}$, $_{FW}$	aft and forward wing
$_L$, $_R$	left and right side
$_O$, $_M$, $_I$	outer, middle, and inner

*Research Engineer, Dynamic Systems and Control Branch, MS 308, Member AIAA
†Research Engineer, Aeroelasticity Branch, MS 340, Senior Member AIAA
‡Research Engineer, Dynamic Systems and Control Branch, MS 308, Associate Fellow AIAA

I. Introduction

To meet increasing demands for fuel economy gain and noise pollution reduction through improved aerodynamic efficiency, next-generation aircraft are expected to be light weight and highly sophisticated, as indicated by the Green Aircraft Challenge and the NASA Fundamental Aeronautics Program, for example. As a consequence of these concept aircraft incorporating lighter, larger, and more flexible components, aeroelastic interactions become significant and a substantial effort is needed to understand, model, and mitigate these effects.

Frequency responses are often desired because they are non-parametric linear models that can be identified from measured data and do not require prior knowledge of the model structure. In aeroelastic wind tunnel tests, each control surface on the test article is sequentially excited using a frequency sweep, which consists of a sinusoid waveform with a continuously increasing frequency. After the test has finished and data has been collected, frequency responses between each input and output are computed using Welch's method or a similar technique;[1–3] however, this method has a number of drawbacks. Frequency sweeps continuously transition through the frequencies, which excites transient responses and limits the amount of excitation at any given frequency. The input amplitude is designed according to the output response amplitude at resonant frequencies, which results in lower signal-to-noise ratios when exciting other frequencies. For rigid-body models, long record lengths of 90–120 seconds of data are needed for good results.[2] In aeroservoelastic problems, there are numerous inputs and outputs due to the spatially distributed nature of structural dynamics, which can further lead to long test times. While several commercial packages exist to help automate the analysis,[2,4] numerous engineering judgments are needed to estimate frequency responses, including selection of window number, size, shape, and overlap, to mitigate problems due to finite record lengths, low excitations, and measurement noise. Finally, there is no direct measurement of uncertainty for the estimated frequency response; instead, the coherence is used, which evaluates the degree of linearity between an input and output.

A new method for estimating frequency responses and their uncertainties efficiently and in real time is presented here. The method uses orthogonal phase-optimized multi-sine inputs to excite all control surfaces simultaneously, uniquely, and over a specified frequency range of interest. The Fourier transform converts output data into the frequency domain, where a least-squares technique extracts the relative magnitude and phase angle, as well as the associated uncertainties. A recursive version of the Fourier transform is also implemented to perform the estimation in real time as the data streams, rather than after the test has been conducted. This method removes many of the engineering judgments needed in frequency response estimation and directly estimates the uncertainty. Consequently, this method can change the way in which wind tunnel tests occur: data is streamed until frequency response estimates have reached prescribed uncertainty levels, at which time the test is stopped. This procedure would help diagnose problems and minimize time spent conducting wind tunnel tests. The method is applied here to previous aeroelastic wind-tunnel test data for the Joined-Wing SensorCraft, a vehicle designed for studying aeroelastic effects using a large number of control surfaces and embedded sensors. The method is similar to other real-time frequency response methods developed recently[5,6] but mitigates problems associated with spectral leakage and evaluation of the Fourier transform at non-integer multiples of the excitation periods. The method also differs from a real-time technique that uses a known model structure to estimate parameters, such as stability and control derivatives, using the equation-error approach in the frequency domain.[7,8] In addition to computing frequency responses from wind-tunnel data, this technique is applicable to identifying aircraft flight dynamics and pilot models, aiding in accident investigations, and adjudicating adaptive control laws with simple metrics.

In section II, the multi-sine input design is summarized, the frequency response and uncertainty estimation is detailed, and an illustrative example using an F-16 nonlinear simulation is presented. Afterwards in section III, the Joined-Wing SensorCraft test article and wind tunnel setup are discussed. In section IV, results are presented for bending strain gage measurements due to symmetric control surface deflections. The input design, aircraft simulation, and data analysis presented in this work were performed using a MATLAB toolbox called System IDentification Programs for AirCraft (SIDPAC). Developed at NASA Langley Research Center, this software is continually improved and is publicly available.[3]

II. Method

This section is divided into five parts. The first part summarizes the design of the excitation inputs. The second and third parts present the algorithm for estimating the frequency response and its uncertainty from measured data. In the fourth part, the method is made recursive for real-time evaluation. The final part illustrates the method using an F-16 nonlinear simulation.

A. Multi-Sine Excitation Design

Orthogonal, phase-optimized multi-sine perturbation inputs have been developed to excite targeted dynamics of multiple-input, multiple-output systems in an efficient manner for system identification. The design of these inputs is documented in detail by Morelli[7,9] and briefly summarized here. Each input is the summation of sinusoids

$$u_j(t) = \sum_{k \in K_j} a_k \sin\left(\frac{2\pi k}{T} t + \phi_k\right) \tag{1}$$

where K_j is the set of indices for the jth input, a_k is the amplitude, T is the record length, $\omega_k = 2\pi k/T$ is the excitation frequency, and ϕ_k is the phase angle. The record length determines the fundamental frequency of the input, of which the excitation frequencies are integer multiples. The excitation frequencies may be assigned to the inputs and their sinusoid amplitudes selected arbitrarily. The full set of n_ω total excitation frequency indices K is the union of the disjoint sets K_j. Phase angles are determined using a simplex optimization to minimize the peak-to-peak amplitude of each input.

Superposition of sinusoid inputs minimizes the record length needed for a given amount of excitation since all frequencies are excited at the same time, in contrast to traditional frequency sweeps where the frequencies are continuously changed. Additionally, the sinusoids are harmonics and therefore orthogonal so that all input channels can be excited simultaneously for system identification without correlating the responses, which further reduces required data record lengths. Assignment of excitation frequencies to input channels and selection of sinusoid amplitudes can be tailored to excite or avoid specific spectral bands and to meet signal-to-noise requirements. The optimized phase angles result in small perturbation responses from nominal conditions, which are desired for identifying linear models including frequency responses. Furthermore, applying all sinusoids simultaneously permits development of the steady-state response, which is consistent with the original sine-dwell technique.

These inputs have led to good modeling results in a variety of unconventional flight conditions such as post-stall, high side-slip angle, and hypersonic flight.[7,10] Excitations are added just before software actuator limiters on control surface deflection angle and rate to maintain low correlation amidst pilot inputs and feedback control. A linear system under this excitation will yield the steady-state responses

$$y_i(t) = \sum_{k \in K} b_k \sin\left(\frac{2\pi k}{T} t + \psi_k\right) \tag{2}$$

which are sinusoids of the same frequencies but different amplitudes and phase angles. For a system with multiple inputs, each output potentially contains dynamic response from all the inputs.

B. Frequency Response Estimation

To estimate the frequency response, output measurements are first converted from the time domain into the frequency domain. The finite Fourier transform of the output, using the first t seconds of data, is

$$\tilde{y}(t, \omega) = \int_0^t y(\tau) e^{-j\omega\tau} d\tau \tag{3}$$

where ω is the radian frequency. In applications where the sampling rates are an order of magnitude larger than the frequencies of interest, Eq. (3) can be approximated by the discretization

$$\tilde{y}(n\Delta t, \omega) \simeq \sum_{m=0}^{n-1} y(m\Delta t) e^{-j\omega n \Delta t} \Delta t, \qquad n = 0, 1, \ldots, T/\Delta t \tag{4}$$

where n is the time index and Δt is the sampling interval.

The Fourier transform of the steady-state response has an analytical solution, found by substituting Eq. (2) into Eq. (3), writing the sinusoid in terms of complex exponentials, and integrating by parts. The result is

$$\begin{aligned}\tilde{y}(t,\omega) &= \sum_{k\in K} \nu_k \cdot (f_k + jg_k) + \xi_k \cdot (f_k - jg_k) \\ &= \sum_{k\in K} (\nu_k + \xi_k) \cdot f_k + j(\nu_k - \xi_k) \cdot g_k \end{aligned} \tag{5}$$

where

$$\begin{aligned}\nu_k &= \frac{1}{2}\left(\frac{1}{\omega-\omega_k}\right)\left(e^{-j(\omega-\omega_k)t} - 1\right) \\ \xi_k &= \frac{1}{2}\left(\frac{1}{\omega+\omega_k}\right)\left(1 - e^{-j(\omega+\omega_k)t}\right) \\ f_k &= b_k e^{j\psi_k} \\ g_k &= b_k e^{-j\psi_k} \end{aligned} \tag{6}$$

and valid at any time t. Equation (5) is the analytical representation of the steady-state output Fourier transform of a linear system subject to multi-sine inputs and is dependent on the excitation frequencies, output amplitudes and phase angles, and the record length. If Eq. (5) is evaluated at $\omega = \omega_k$, the formula for ν_k takes the indeterminant form $0/0$ and

$$\lim_{\omega\to\omega_k} \nu_k = -jt/2 \tag{7}$$

should be used.

Equation (4) is used to compute numerical samples of the output Fourier transform, which is represented analytically by Eq. (5). The unknown output amplitude and phase angles can be estimated using the least-squares framework

$$\mathbf{y} = \mathbf{X}\boldsymbol{\theta} \tag{8}$$

where $\mathbf{y}$ is the vector of n_f numerical evaluations of the Fourier transform,

$$\mathbf{X} = \left[\begin{array}{cccc|cccc} (\boldsymbol{\nu}_1 + \boldsymbol{\xi}_1) & (\boldsymbol{\nu}_2 + \boldsymbol{\xi}_2) & \ldots & (\boldsymbol{\nu}_{n_\omega} + \boldsymbol{\xi}_{n_\omega}) & j(\boldsymbol{\nu}_1 - \boldsymbol{\xi}_1) & j(\boldsymbol{\nu}_2 - \boldsymbol{\xi}_2) & \ldots & j(\boldsymbol{\nu}_{n_\omega} - \boldsymbol{\xi}_{n_\omega}) \end{array}\right] \tag{9}$$

is an n_f by $2n_\omega$ matrix of regressors, and

$$\boldsymbol{\theta} = \left[\begin{array}{cccc|cccc} f_1 & f_2 & \ldots & f_{n_\omega} & g_1 & g_2 & \ldots & g_{n_\omega} \end{array}\right]^T \tag{10}$$

is a vector of $2n_\omega$ unknown variables. To keep the least-squares problem well-posed, at least two evaluations of the Fourier transform are needed for each excitation frequency; i.e., $n_f \geq 2n_\omega$. The least-squares solution is

$$\hat{\boldsymbol{\theta}} = \Re\{\mathbf{X}^\dagger\mathbf{X}\}^{-1}\Re\{\mathbf{X}^\dagger\mathbf{y}\} \tag{11}$$

where $\Re$ denotes the real part. At least $2\pi/\Delta\omega$ seconds of data are needed so that $\Re\{\mathbf{X}^\dagger\mathbf{X}\}$ is well-conditioned for matrix inversion, where $\Delta\omega$ is the smallest increment in excitation frequency. The output amplitude and phase angle estimates are extracted from Eq. (11) as

$$\begin{aligned}\hat{b}_k &= \sqrt{\hat{f}_k^2 + \hat{g}_k^2} \\ \hat{\psi}_k &= \arctan(\hat{g}_k/\hat{f}_k). \end{aligned} \tag{12}$$

Then given amplitudes and phase angles for the inputs and outputs, the frequency response is computed in terms of its relative magnitude and phase angle

$$\begin{aligned}\|\hat{G}(j\omega_k)\| &= \hat{b}_k/a_k \\ \angle\hat{G}(j\omega_k) &= \hat{\psi}_k - \phi_k. \end{aligned} \tag{13}$$

Estimation of amplitudes and phases is only required for the output because the input amplitude and phase are known from design; however, if actuators introduce significant dynamics or if surface deflection measurements are available, the same procedure can be used to estimate amplitudes and phase angles for the input. This method mitigates errors from spectral leakage and evaluating the Fourier transform at non-integer multiples of the excitation periods because the structure of the steady-state output Fourier transform is known.[5]

C. Uncertainty Analysis

Uncertainty in the frequency response is useful for indicating the quality of the estimation. Assuming a constant variance of the residual $\mathbf{y} - \mathbf{X}\hat{\boldsymbol{\theta}}$, the least-squares solution Eq. (11) has the covariance matrix

$$\boldsymbol{\Sigma}(\hat{\boldsymbol{\theta}}) = \left[\begin{array}{cccc:cccc} \sigma^2_{f_1} & \sigma^2_{f_1,f_2} & \dots & \sigma^2_{f_1,f_{n_\omega}} & \sigma^2_{f_1,g_1} & \sigma^2_{f_1,g_2} & \dots & \sigma^2_{f_1,g_{n_\omega}} \\ \sigma^2_{f_2,f_1} & \sigma^2_{f_2} & \dots & \sigma^2_{f_2,f_{n_\omega}} & \sigma^2_{f_2,g_1} & \sigma^2_{f_2,g_2} & \dots & \sigma^2_{f_2,g_{n_\omega}} \\ \vdots & \vdots & \ddots & \vdots & \vdots & \vdots & \ddots & \vdots \\ \sigma^2_{f_{n_\omega},f_1} & \sigma^2_{f_{n_\omega},f_2} & \dots & \sigma^2_{f_{n_\omega}} & \sigma^2_{f_{n_\omega},g_1} & \sigma^2_{f_{n_\omega},g_2} & \dots & \sigma^2_{f_{n_\omega},g_{n_\omega}} \\ \hdashline \sigma^2_{g_1,f_1} & \sigma^2_{g_1,f_2} & \dots & \sigma^2_{g_1,f_{n_\omega}} & \sigma^2_{g_1} & \sigma^2_{g_1,g_2} & \dots & \sigma^2_{g_1,g_{n_\omega}} \\ \sigma^2_{g_2,f_1} & \sigma^2_{g_2,f_2} & \dots & \sigma^2_{g_2,f_{n_\omega}} & \sigma^2_{g_2,g_1} & \sigma^2_{g_2} & \dots & \sigma^2_{g_2,g_{n_\omega}} \\ \vdots & \vdots & \ddots & \vdots & \vdots & \vdots & \ddots & \vdots \\ \sigma^2_{g_{n_\omega},f_1} & \sigma^2_{g_{n_\omega},f_2} & \dots & \sigma^2_{g_{n_\omega}} & \sigma^2_{g_{n_\omega},g_1} & \sigma^2_{g_{n_\omega},g_2} & \dots & \sigma^2_{g_{n_\omega},g_{n_\omega}} \end{array}\right] = \sigma^2 \Re\{\mathbf{X}^\dagger \mathbf{X}\}^{-1} \tag{14}$$

for which the fit error variance estimate is

$$\hat{\sigma}^2 = \frac{(\mathbf{y} - \mathbf{X}\hat{\boldsymbol{\theta}})^\dagger (\mathbf{y} - \mathbf{X}\hat{\boldsymbol{\theta}})}{n_f - 2n_\omega} \tag{15}$$

and is valid when the problem is over-determined; i.e., $n_f > 2n_\omega$.

The uncertainty in the estimation is propagated using the least-squares covariance matrix and first-order Taylor series approximations. The output amplitude uncertainty is

$$\begin{aligned} \hat{\sigma}^2_{b_k} &= \left(\frac{\partial \hat{b}_k}{\partial \hat{f}_k}\right)^2 \hat{\sigma}^2_{f_k} + \left(\frac{\partial \hat{b}_k}{\partial \hat{g}_k}\right)^2 \hat{\sigma}^2_{g_k} + 2\left(\frac{\partial \hat{b}_k}{\partial \hat{f}_k}\right)\left(\frac{\partial \hat{b}_k}{\partial \hat{g}_k}\right) \hat{\sigma}^2_{f_k,g_k} \\ &= (\hat{f}_k^2 + \hat{g}_k^2)^{-1} (\hat{f}_k^2 \hat{\sigma}^2_{f_k} + \hat{g}_k^2 \hat{\sigma}^2_{g_k} + 2\hat{f}_k^2 \hat{g}_k^2 \hat{\sigma}^2_{f_k g_k}) \end{aligned} \tag{16}$$

and similarly

$$\hat{\sigma}^2_{\psi_k} = (\hat{f}_k^2 + \hat{g}_k^2)^{-2} (\hat{g}_k^2 \hat{\sigma}^2_{f_k} + \hat{f}_k^2 \hat{\sigma}^2_{g_k} - 2\hat{f}_k^2 \hat{g}_k^2 \hat{\sigma}^2_{f_k g_k}) \tag{17}$$

for the output phase angle uncertainty. The uncertainties can then be propagated through the the relative magnitude and phase angle Eq. (13) as

$$\begin{aligned} \hat{\sigma}^2_{\|G(j\omega_k)\|} &= \left(\frac{\hat{b}_k^2}{\hat{a}_k^4}\right) \hat{\sigma}^2_{a_k} + \left(\frac{1}{\hat{a}_k^2}\right) \hat{\sigma}^2_{b_k} - 2\left(\frac{\hat{b}_k}{\hat{a}_k^3}\right) \hat{\sigma}^2_{a_k b_k} \\ \hat{\sigma}^2_{\angle G(j\omega_k)} &= \hat{\sigma}^2_{\phi_k} + \hat{\sigma}^2_{\psi_k} - 2\hat{\sigma}^2_{\phi_k \psi_k}. \end{aligned} \tag{18}$$

The uncertainties of the input amplitudes and phase angles can be neglected because they are either null, due to knowledge of the input design, or negligible, as system identification experiments are devised to have good measurements of the input.

Accuracy of error bounds can be improved by obtaining uncertainties on the input and output measurements, and then propagating the error through the Fourier transforms[11] and applying a weighted least-squares solution in place of Eq. (8); however, it was found that this method adds significant computation time and was not used.

D. Recursive Formulation

As presented above, the method is used in batch execution after all the experimental data have been collected. A reformulation can alternatively be used to update frequency responses in real time as the experiment is conducted. The output Fourier transform can be made recursive as

$$\tilde{y}(n\Delta t, \omega) = \tilde{y}(n\Delta t - \Delta t, \omega) + y(n\Delta t)e^{-j\omega n\Delta t}\Delta t. \tag{19}$$

For typical record lengths, Fourier transforms may be initiated to zero with negligible losses in accuracy. Fourier transforms should be updated with each new data sample, but frequency responses may be estimated at any rate desired, provided enough data has been collected to avoid singularities in the least-squares estimation.

E. Illustrative Example

The method is demonstrated using the flight dynamics of the F-16 fighter aircraft. A nonlinear simulation, adapted from Stevens and Lewis,[12] is included in SIDPAC and contains routines for computing linear models using central finite differences. The aircraft was trimmed for straight and level flight at 10,000 ft altitude, 0.24 throttle, 617 ft/s airspeed, and 2.0 deg angle of attack. Numerical linearization resulted in the transfer function

$$\frac{\Delta q(s)}{\Delta \delta_e(s)} = \frac{-12.10(s + 0.865)}{(s^2 + 2.461s + 7.451)} \tag{20}$$

describing the elevator to pitch rate perturbation dynamics with only the longitudinal states and the application of the short period approximation.[13]

The nonlinear simulation was excited with the 20 second multi-sine elevator perturbation described in Table 1, which has a 2.0 deg peak-to-peak amplitude and frequencies between 0.1 Hz and 2.0 Hz in 0.1 Hz increments. Figure 1 shows measurements of the elevator, angle of attack, and pitch rate, which were corrupted with white Gaussian noise sequences resulting in 20:1, 5:1, and 5:1 signal-to-noise levels, respectively.

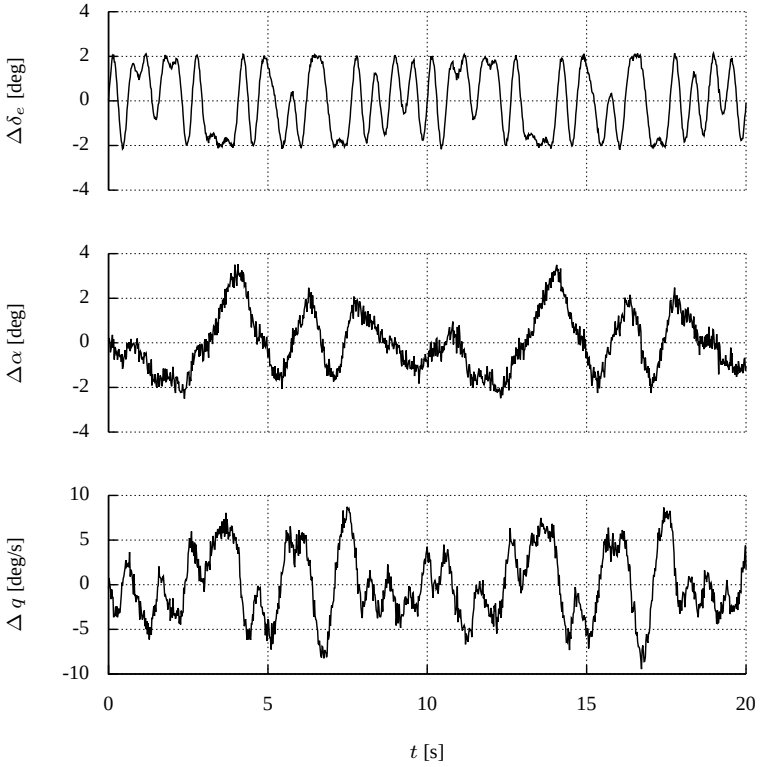

Figure 1. Simulated F-16 data for time-invariant modeling

Table 1. Multi-sine F-16 elevator perturbation input parameters ($T = 20$ s)

Index k	Amplitude a_k [deg]	Frequency k/T [Hz]	Phase Angle ϕ_k [rad]
2	0.45	0.1	1.34
4	0.45	0.2	0.33
6	0.45	0.3	4.35
8	0.45	0.4	3.30
10	0.45	0.5	6.03
12	0.45	0.6	2.86
14	0.45	0.7	4.43
16	0.45	0.8	6.20
18	0.45	0.9	2.70
20	0.45	1.0	2.10
22	0.45	1.1	6.15
24	0.45	1.2	0.80
26	0.45	1.3	4.90
28	0.45	1.4	2.06
30	0.45	1.5	5.38
32	0.45	1.6	5.56
34	0.45	1.7	0.18
36	0.45	1.8	0.59
38	0.45	1.9	0.84
40	0.45	2.0	4.84

The fitting of the input elevator and output pitch rate Fourier transforms at 20 seconds are shown in Figures 2(a) and 2(b). The fittings match well, although larger errors in the pitch rate estimation are due to increased noise and the presence of the transient response in the Fourier transform. Figures 2(c) and 2(d) show the magnitude and phase angle estimates and 2σ error bounds at 20 seconds, along with the true solution. The frequency response estimates are close to and in statistical agreement with the true frequency response. The error bounds are smallest near the short period mode resonance at 2.73 rad/s, where there are good excitations and high signal-to-noise ratios. At lower frequencies there are fewer cycles of excitation, and at higher frequencies there are lower signal-to-noise ratios. The error bounds are conservative because transient solutions are present in the pitch rate response, error in the Fourier transform is not accounted taken into account, and the minimal number of regressors are used in the least-squares estimator to save computation time. Figures 2(e) and 2(f) show the real-time estimates of the magnitude and phase angle along with the final estimates and true frequency response. Although Fourier transforms were recursively estimated throughout the maneuver, frequency response estimates were not initiated until 10 seconds to ensure that $\Re\{\mathbf{X}^\dagger\mathbf{X}\}$ was well-conditioned for matrix inversion. Once this condition was met, frequency response estimates quickly converged to the true values.

III. Wind-Tunnel Model and Test Setup

The Joined-Wing SensorCraft was developed to support the Aerodynamic Efficiency Improvement Program led by the Air Force Research Laboratory.[14] The goals were to demonstrate stable flight under reduced static stability, measure stability margins during flight, and alleviate gust loadings on the first two structural modes. The model was designed, constructed, and tested by Boeing, the United States Air Force, NextGen Aeronautics, Millenium Dynamics, and NASA.[15–20]

The wind-tunnel test article is an aeroelastically-scaled 8% model of the Boeing Joined-Wing SensorCraft concept. Bending and torsional stiffness were scaled for the wings and boom using spar design, and the mass distribution was scaled using lead weights. The model consists of a fuselage, two aft-swept wings, two forward-swept wings, and a tail boom. Figure 3(a) shows a planform view schematic indicating locations of imbedded instrumentation. There are 13 independent control surfaces which are driven by hydraulic actuators and measured using rotational variable differential transformers. Embedded in the wings are 14 accelerometers, 15 bending strain gauges, 5 leading-edge stagnation point sensors, and 5 rate gyros.

Several Joined-Wing SensorCraft configurations were tested in the NASA Langley Transonic Dynamics Tunnel. The test medium tetrafluoroethane R-134a was used for similitude scaling. The test article was mounted on the device shown in Figure 3(b), which afforded optional pitch and plunge degrees of freedom. Testing occurred at 0.22 Mach with a dynamic pressure of 51 lb/ft^2. Data was recorded using a dSPACE data aquisition system and decimated to 500 Hz for analysis. Multi-sine excitation perturbations were added to trim surface deflection commands using LabVIEW.

Highlighted here is test number 614, run number 35, where the pitch and plunge motions were constrained and only the aeroelastic deflections were free. Control surfaces were commanded symmetrically about the center line. The modeling inputs are the averaged deflection measurements

$$u_{cd} = \frac{1}{2}(\delta_{cRd} + \delta_{cLd}) \tag{21}$$

where δ is the control surface deflection, $c \in \{FW, AW\}$ denotes forward and aft wing, $\{R, L\}$ denote right and left wing, and $d \in \{O, M, I\}$ denotes outer, middle, and inner surfaces. Six multi-sine inputs were used to excite all 12 surfaces simultaneously, each with a record length of 100 seconds and containing 83 frequencies between 0.01 Hz and 9.95 Hz.[21] The relatively long duration was needed to accomodate the dense frequency gridding desired for aeroelastic analysis. The commanded perturbation deflections had root mean squared values of 1.99 deg. Excitation frequencies were distributed in an alternating fashion to the input channels and with uniform power. An optimization of the phase angles was prohibitive for such a large number of inputs and excitation frequencies, so the phase angles were generated at random and iterated until low peak-to-peak amplitudes were obtained. Frequency responses from control surface deflections to sensor outputs were estimated; however, in the interest of space, only the forward right wing outer strain due to control surface deflection frequency response will be presented here; i.e., 6 inputs and 1 output. A limited time slice sample of model inputs and bending strain gauge outputs is shown in Figure 4. Although ideally the output responses should be symmetric about the center line, differences indicate that time histories of

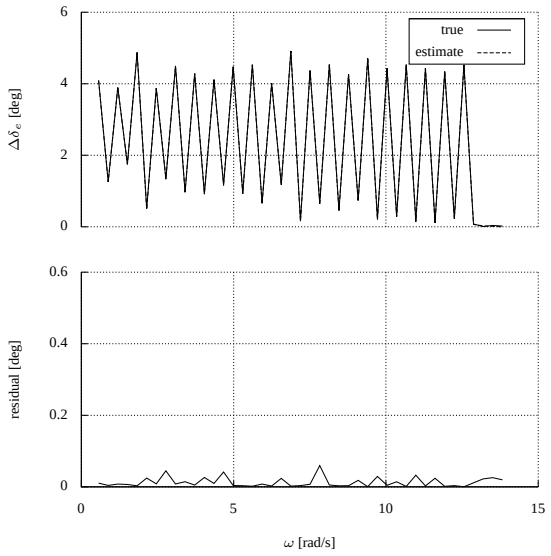

(a) input Fourier transform fitting at 20 s

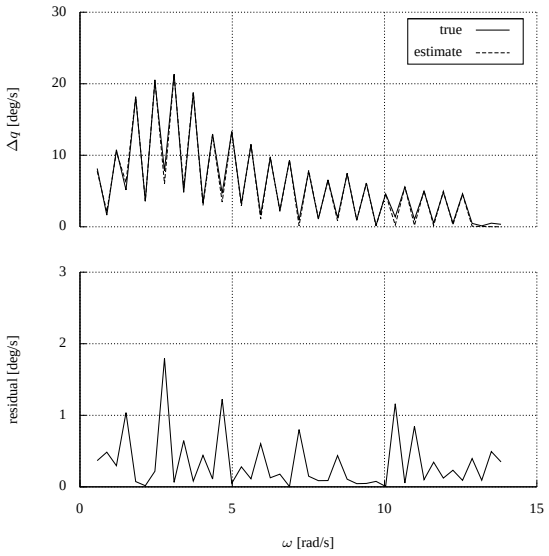

(b) output Fourier transform fitting at 20 s

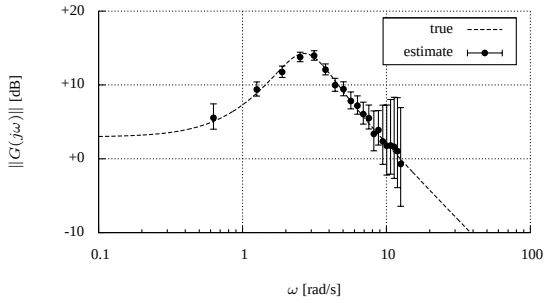

(c) magnitude and 2σ errors at 20 s

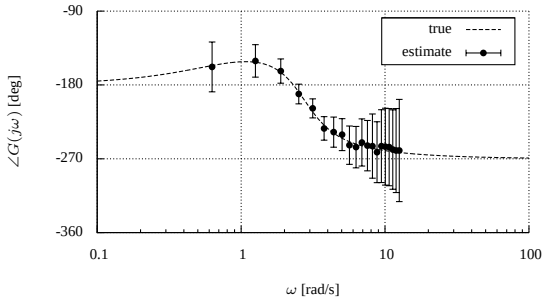

(d) phase angle 2σ errors at 20 s

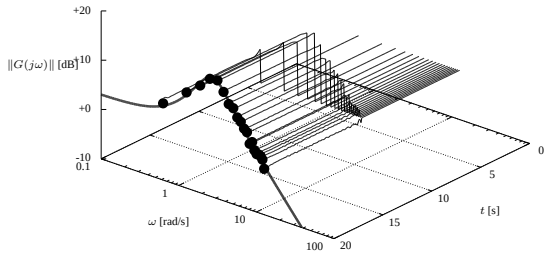

(e) magnitude evolution

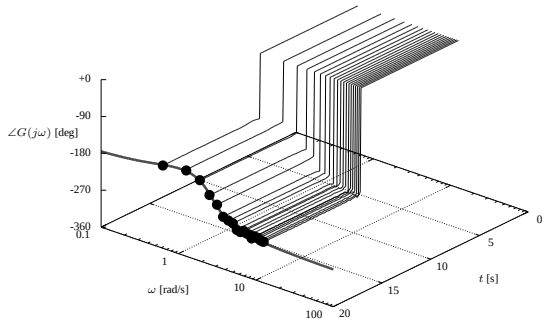

(f) phase angle evolution

Figure 2. F-16 elevator to pitch rate frequency response estimation

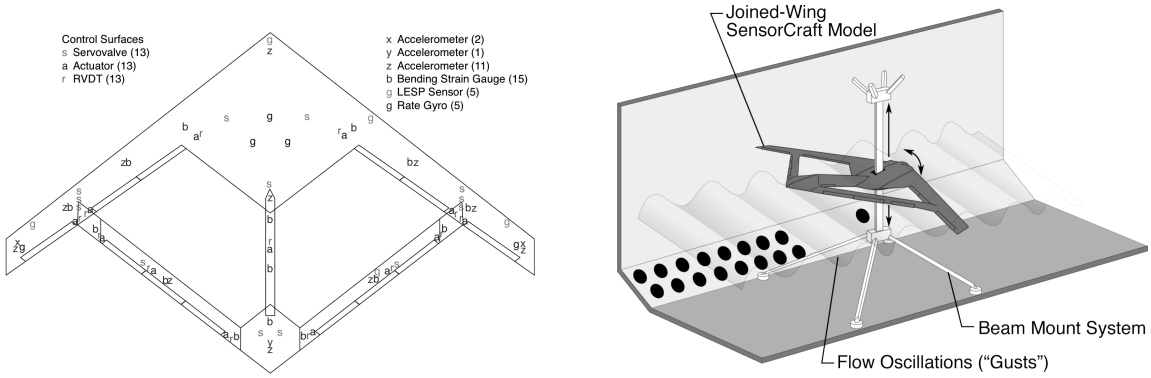

(a) planform schematic

(b) testing configuration

Figure 3. Joined-wing SensorCraft schematic and wind tunnel test setup[20]

the outputs should not be averaged together; rather, each frequency response should be estimated and then averaged between the left and right wings.

As both the actuator command and responses were available for all 12 flaps, system identification was performed to acquire actuator models. Figure 5(a) shows a limited time slice sample of the command to and response of the forward wing, outer control surface on the left side. Quantization effects are evident in the command, as well as amplitude and phase distortions in the response. The equation-error parameter estimation method in the frequency domain[3] was used to fit a first-order model to the data, as shown in Figure 5(b). Coefficients of determination were above 0.99 and estimated parameter standard errors were below 0.2%, implying an excellent match. The spread of identified frequency responses is shown in Figure 5(c) and indicates the actuators had a conservative -3 dB bandwidth of 20 Hz, which is twice the highest excitation frequency. Despite some magnitude and phase angle distortions, the control surface deflections have mutual correlation coefficients below 0.001, suggesting that while they were not orthogonal, they were nearly so and served well for system identification.

IV. Results

The test article was fixed on the mounting with constrained pitch and plunge degrees of freedom so that only the aeroelastic degrees of freedom were excited. The 6 multi-sine perturbation excitations were injected at the actuators to deflect the twelve control surfaces in a symmetric manner while sensor measurements were recorded. After the test was completed, the real-time frequency response algorithm described was applied to estimate the dynamics between the symmetric surface deflections and the outer bending strain on the left side forward wing.

Frequency response estimates obtained at the end of the manuever are shown in Figure 6; forward wing surface deflection frequency responses are shown on the left column, and aft wing surface deflection frequency responses are on the right column. Consistent with previous findings, the lowest two aeroelastic modes are at 32.7 rad/s and 63.5 rad/s.[21] The forward wing outer surface forcing had the highest signal-to-noise ratio due to the high strains recorded from the co-located actuation and thus the most accurate frequency response estimate, despite the fact that all control surfaces were moving simultaneously. Moving inboard along the wing and to the aft wing, the frequency responses from the surface deflections had lower strains and lower signal-to-noise ratios, resulting in biased frequency response estimates and larger uncertainties.

The evolution of real-time magnitude and phase angle estimates are shown in Figures 7 and 8. Each trace shows the evolution of a magnitude or phase angle estimate at a particular excitation frequency. Frequency response estimates were only computed after 50 seconds because that time is needed to ensure that the columns of the regressor matrix are linearly independent and the least-squares problem is well-posed. The 360 deg jumps in the phase angle estimates are an imposed constraint that the lowest phase angle remain within $[0, 360)$ deg because this is a causal system. The magnitude estimates of the forward wing outer surface deflection to strain converged immediately after 50 seconds, with the exception of estimates around

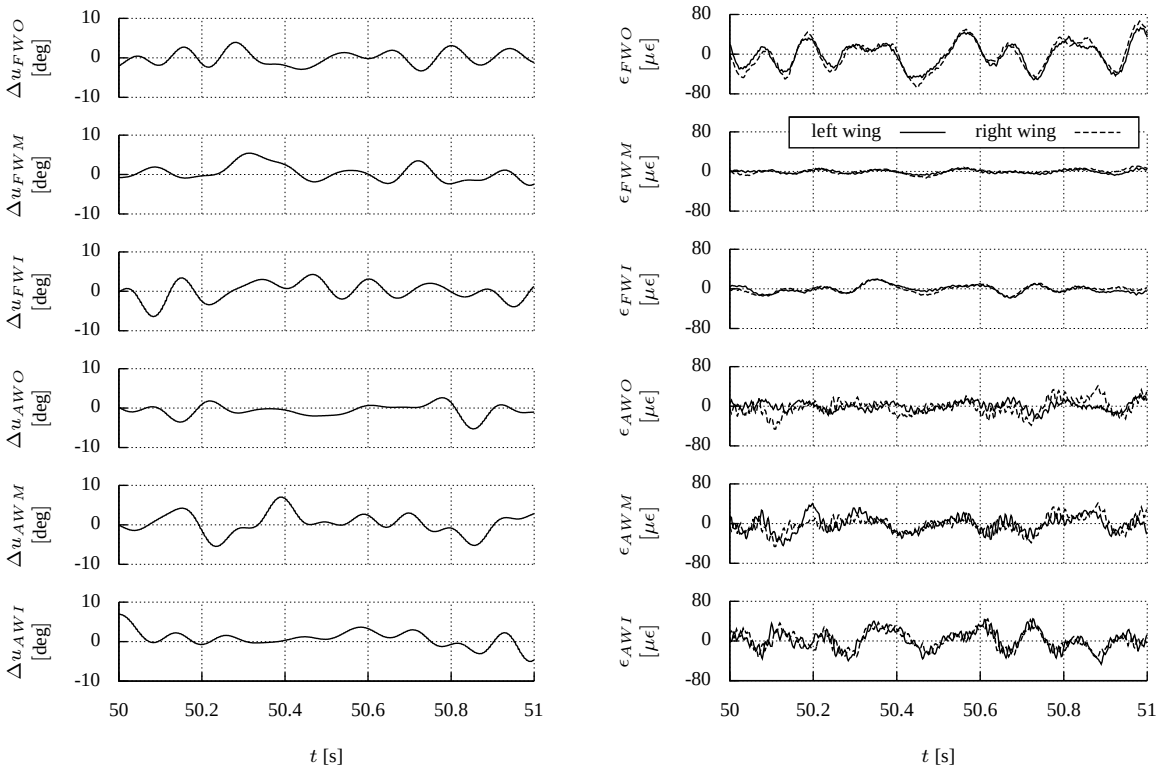

(a) model inputs

(b) bending strain gauge outputs

Figure 4. Time slice sample of measurements

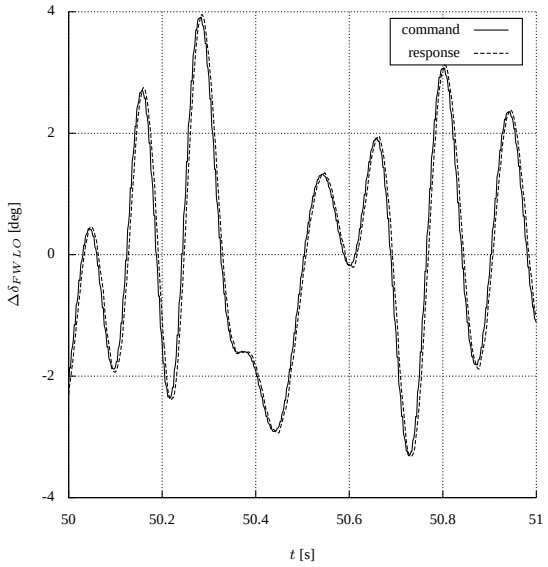

(a) left front wing outer control surface deflection command and response

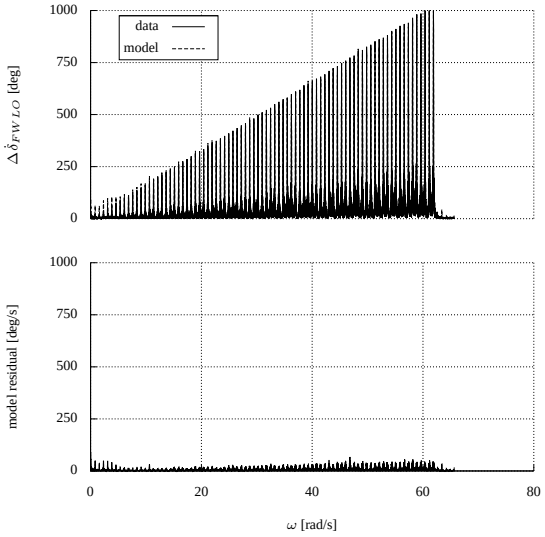

(b) fit of model to response velocity data using equation-error in the frequency domain

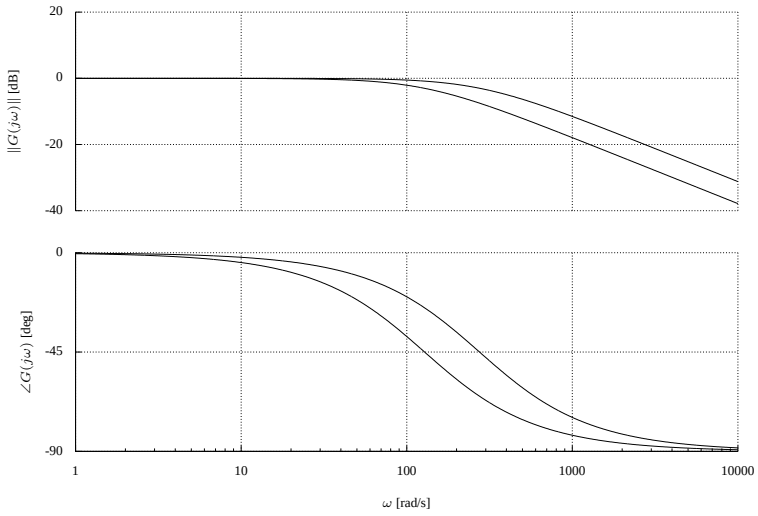

(c) spread of identified actuator frequency responses

Figure 5. Identified control surface actuator models from command and response measurements

the transmission zero at 48 rad/s. Other magnitude frequency response estimates converged in the higher frequency range where the signal-to-noise ratios were better. Similarly, the phase angle for the strain due to deflection of the forward wing outer surface converged quickly after estimation began, and similarly for the other forward wing surface deflections. The phase angle estimates from the aft wing surface deflections had lower signal-to-noise ratios and began to converge when the experiment ended at 100 s.

The forward wing outer surface deflection to outer forward wing strain frequency response was estimated well by this method. Frequency responses from the other forward wing surface deflections were estimated well only at higher frequencies where the signal-to-noise ratio was higher. Although the structural modes were evident in the phase angles, frequency responses from the aft wing surfaces were not estimated well because of low signal-to-noise. If this method were applied in real-time as the test was performed, these results would be immediately apparent. If only the co-located frequency response was desired, these results would be sufficient. If the multi-axis frequency responses were also desired, the test engineers could either continue running the tests to accumulate more data, or the amplitudes of the multi-sines could be increased for the inner and aft wing surface deflections. It is possible that with this real-time analysis, the results could be analyzed as the experiment is conducted to expedite changes in the experiment immediately, rather than conducting another test at a later time. This method would save time and money in wind tunnel tests by ensuring that results were of desired accuracy.

V. Conclusion

In this paper, a new method was presented for estimating frequnecy responses from data in real time as an experiment is being conducted. Orthogonal phase-optimized multi-sine inputs were used to compress test durations and excite all control inputs simultaneously and uniquely. A recursive Fourier transform was used to update the spectral content of each output in a computationally-efficient manner. A least-squares method was used to extract amplitude and phase information from these Fourier transforms, which were then used to compute the frequency responses and their uncertainties. The method was demonstrated first using the short period dynamics of an F-16 nonlinear simulation, where good modeling results were obtained using a 20 second maneuver. The method was then demonstrated using Joined-Wing SensorCraft aeroelastic wind tunnel data, where frequency responses between 6 symmetric surface deflection inputs and a bending strain gauge output were estimated from a single 100 second data record. Good results were obtained for the co-located pair, but low signal-to-noise ratios led to poorer results from control surface deflections on the aft wing and closer to the aircraft center line.

A new method was presented for computing frequency responses directly from the data, which bypasses many of the engineering judgements needed in conventional frequency response estimation. A measurement of the frequency response uncertainty is also produced, which describes the quality of the estimate. Furthermore, this process can be made recursive for estimation while the data streams in real time rather than after the experiment has finished.

This work is important because it gives direct feedback on modeling results as an experiment is being conducted. If adequate results have been obtained, the test can be stopped. If adequate results have not yet been obtained, longer test times can be run, larger amplitude inputs can be commanded, or sensor placement can be reconfigured. This real-time knowledge will help diagnose problems and expedite wind tunnel tests to save time and money.

This method is useful in aeroelastic tests where there are numerous control inputs that need to be excited. The multi-sine inputs allow for simultaneous excitation of all input channels, instead of sequential excitation, thereby saving time. The method is useful for aeroelastic wind tunnel tests designed to identify frequency responses, which are then used to design control systems for flutter suppression and load alleviation. Other applications of this method include identifying aircraft or pilot models and stability margins in flight, adjudicating adaptive nonlinear control laws with simple metrics, and alerting pilots and reconfigurable control algorithms to changes in aircraft dynamics due to structural damage, loss-of-control situations, and ice formation.

Acknowledgments

This work was funded under the NASA Subsonic Fixed-Wing Program.

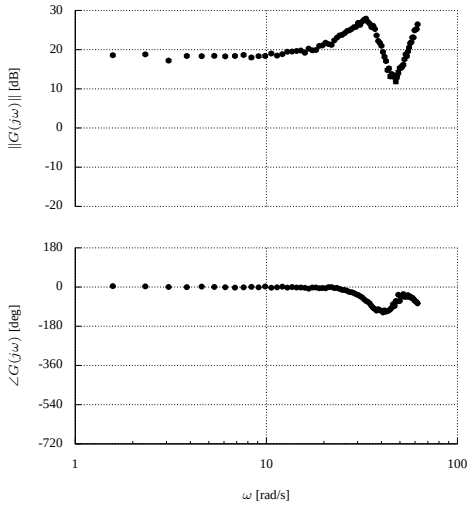

(a) $\Delta u_{FWO} \rightarrow \epsilon_{FWLO}$

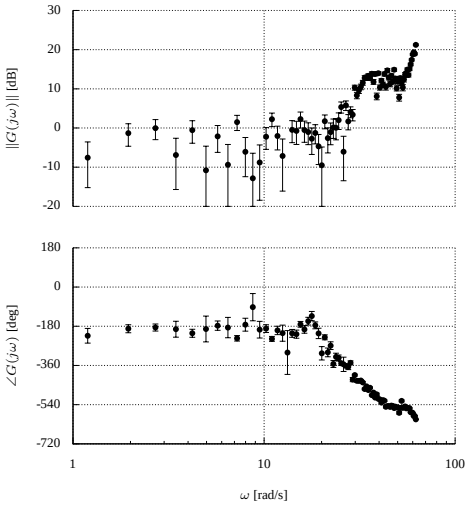

(b) $\Delta u_{AWO} \rightarrow \epsilon_{FWLO}$

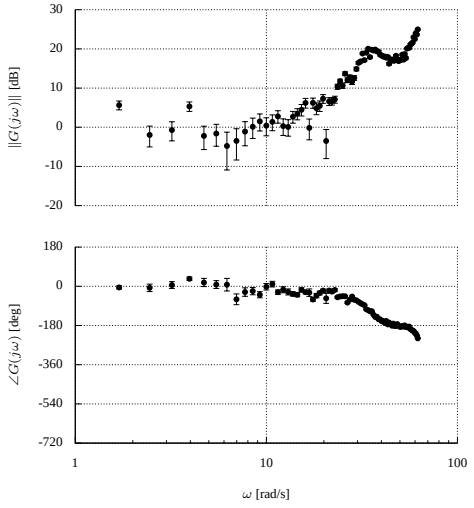

(c) $\Delta u_{FWM} \rightarrow \epsilon_{FWLO}$

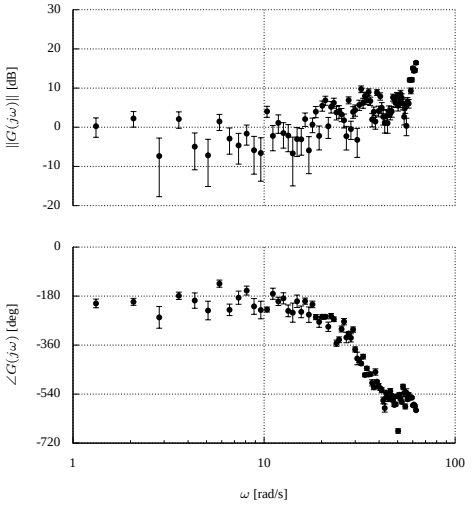

(d) $\Delta u_{AWM} \rightarrow \epsilon_{FWLO}$

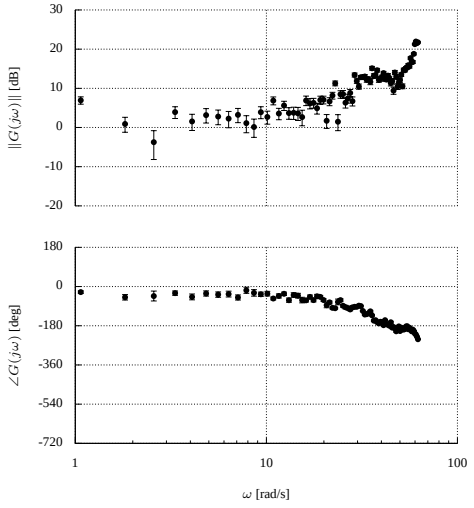

(e) $\Delta u_{FWI} \rightarrow \epsilon_{FWLO}$

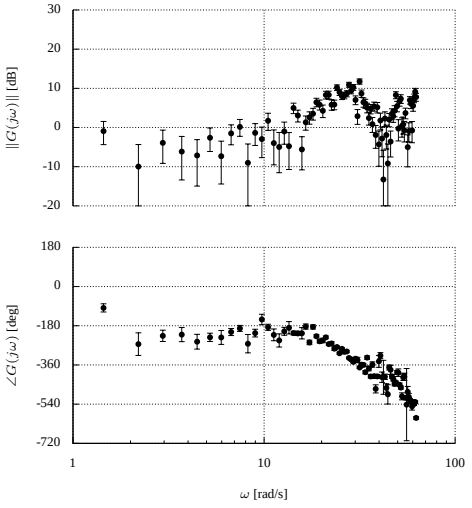

(f) $\Delta u_{AWI} \rightarrow \epsilon_{FWLO}$

Figure 6. Final frequency response estimates and 2σ error bounds at 100 s

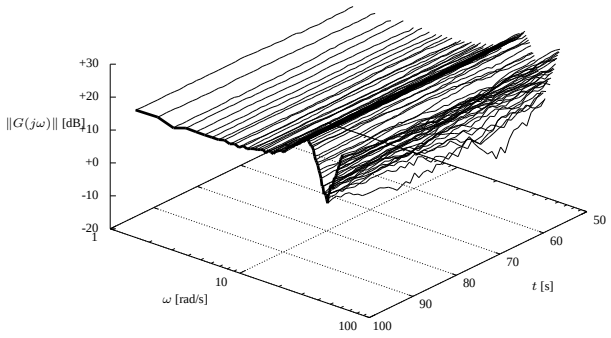

(a) $\Delta u_{FWO} \rightarrow \epsilon_{FWLO}$

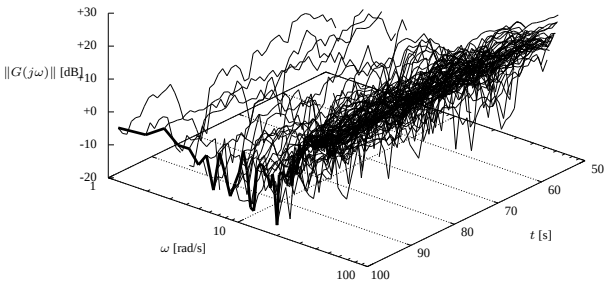

(b) $\Delta u_{AWO} \rightarrow \epsilon_{FWLO}$

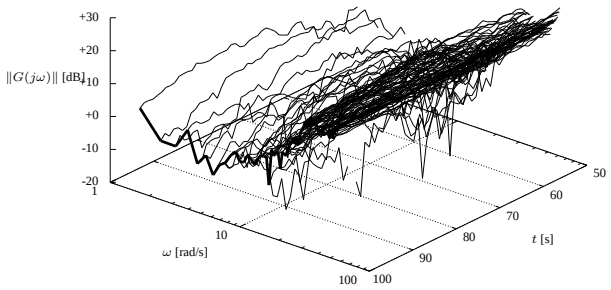

(c) $\Delta u_{FWM} \rightarrow \epsilon_{FWLO}$

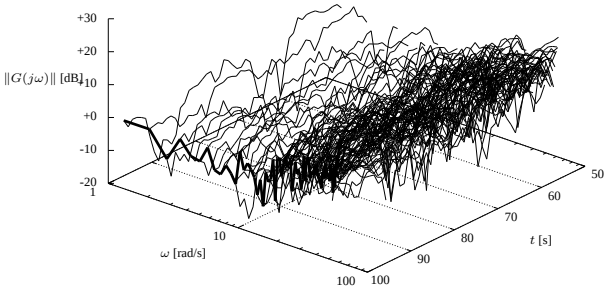

(d) $\Delta u_{AWM} \rightarrow \epsilon_{FWLO}$

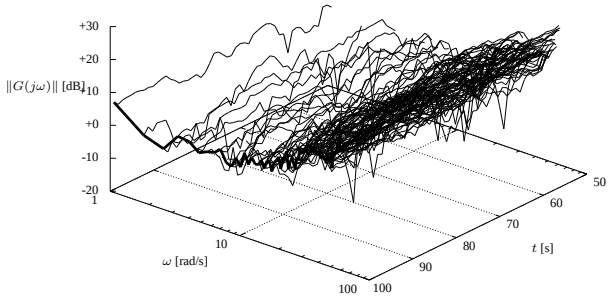

(e) $\Delta u_{FWI} \rightarrow \epsilon_{FWLO}$

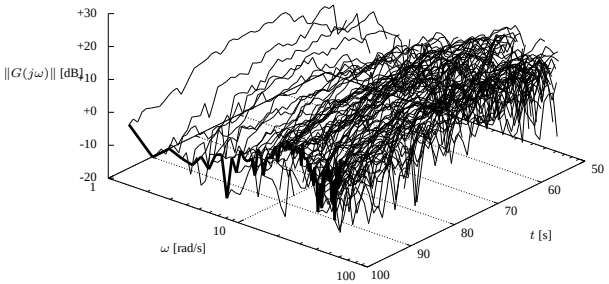

(f) $\Delta u_{AWI} \rightarrow \epsilon_{FWLO}$

Figure 7. Estimated magnitude evolution

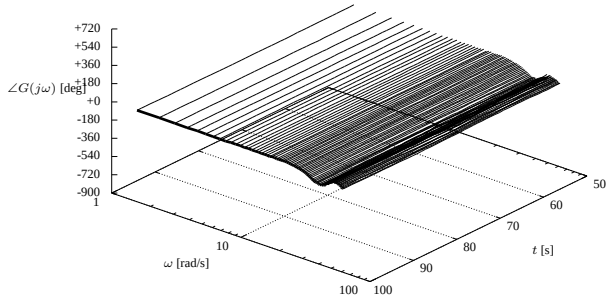

(a) $\Delta u_{FWO} \rightarrow \epsilon_{FWLO}$

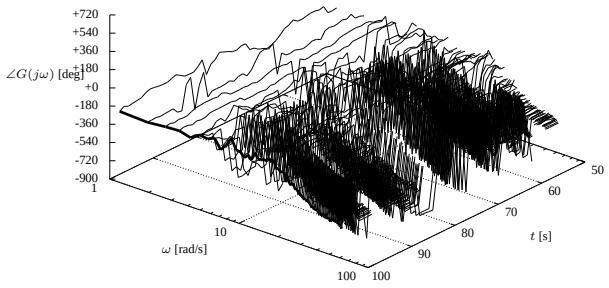

(b) $\Delta u_{AWO} \rightarrow \epsilon_{FWLO}$

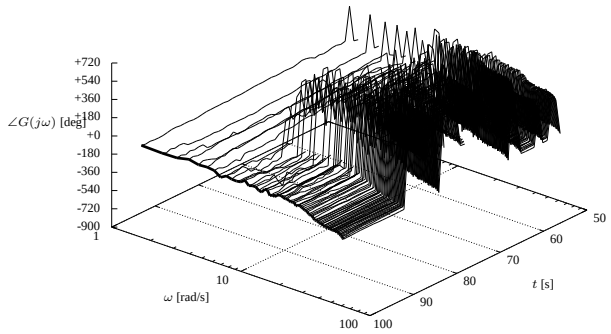

(c) $\Delta u_{FWM} \rightarrow \epsilon_{FWLO}$

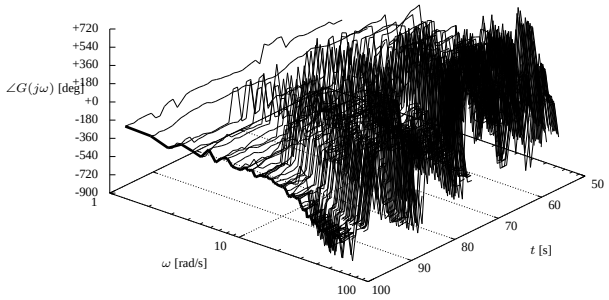

(d) $\Delta u_{AWM} \rightarrow \epsilon_{FWLO}$

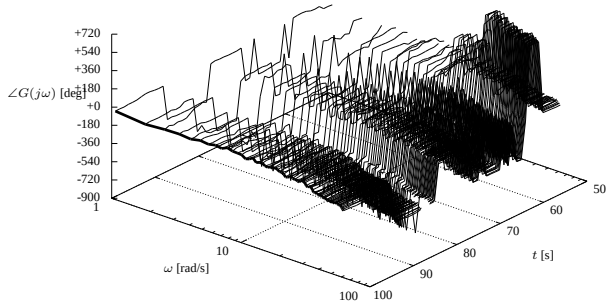

(e) $\Delta u_{FWI} \rightarrow \epsilon_{FWLO}$

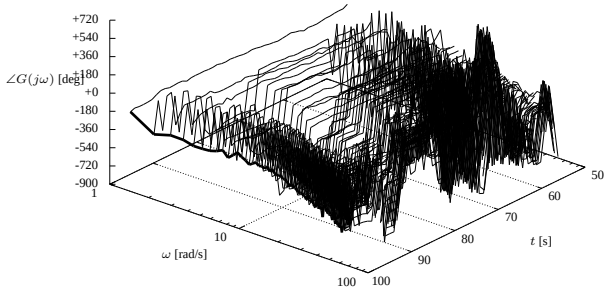

(f) $\Delta u_{AWI} \rightarrow \epsilon_{FWLO}$

Figure 8. Estimated phase angle evolution

References

[1]Bendat, J. and Piersol, A., *Random Data: Analysis and Measurement Procedures*, John Wiley and Sons, 1986.

[2]Tischler, M. and Remple, R., *Aircraft and Rotorcraft System Identification: Engineering Methods with Flight Test Examples*, AIAA, 2006.

[3]Klein, V. and Morelli, E., *Aircraft System Identification: Theory and Practice*, AIAA, 2006.

[4]Ljung, L., *System Identification: Theory for the User*, Prentice Hall, 1999.

[5]Holzel, M. and Morelli, E., "Real-Time Frequency Response Estimation from Flight Data," AIAA Atmospheric Flight Mechanics Conference, AIAA, Portland, OR, August 2011.

[6]Grauer, J. and Morelli, E., "Real-Time Frequency Response Estimation using Multi-Sine Inputs and Recursive Fourier Transform," AIAA Atmospheric Flight Mechanics Conference, AIAA, Minneapolis, MN, August 2012.

[7]Morelli, E., "Flight-Test Experiment Design for Characterizing Stability and Control of Hypersonic Vehicles," *Journal of Guidance, Control, and Dynamics*, Vol. 32, No. 3, May–June 2009, pp. 949–959.

[8]Morelli, E. and Smith, M., "Real-Time Dynamic Modeling: Data Information Requirements and Flight-Test Results," *Journal of Aircraft*, Vol. 46, No. 6, Nov.–Dec. 2009, pp. 1894–1905.

[9]Morelli, E., "Multiple Input Design for Real-Time Parameter Estimation in the Frequency Domain," No. REG–360 in 13th IFAC Conference on System Identification, IFAC, Rotterdam, The Netherlands, August 2003.

[10]Morelli, E., "Flight Test Maneuvers for Efficient Aerodynamic Modeling," No. 2011–6672 in AIAA Atmospheric Flight Mechanics Conference, AIAA, Portland, OR, August 2011.

[11]Forniés-Marquina, J., Letosa, J., García-Gracia, M., and Artacho, J., "Error propagation for the transformation of time domain into frequency domain," *IEEE transactions on magnetics*, Vol. 33, No. 2, March 1997, pp. 1456–1459.

[12]Stevens, B. and Lewis, F., *Aircraft Control and Simulation*, Wiley, 2nd ed., 2003.

[13]McRuer, D., Ashkenas, I., and Graham, D., *Aircraft Dynamics and Automatic Control*, Princeton, 1973.

[14]Martinez, J., Flick, P., Perdzock, J., Dale, G., and Davis, M., "An Overview of SensorCraft Capabilities and Key Enabling Technologies," No. 2008–7185 in AIAA Applied Aerodynamics Conference, AIAA, Honolulu, HI, August 2008.

[15]Reichenbach, E., "Aeroservoelastic Design and Test Validation of the Joined-Wing Sensorcraft," No. 2008–7189 in AIAA Applied Aerodynamics Conference, AIAA, Honolulu, HI, August 2008.

[16]LeDoux, S., Vassberg, J., DeHann, M., and Fatta, G., "Aerodynamic Cruise Design of a Joined Wing SensorCraft," No. 2008–7190 in AIAA Applied Aerodynamics Conference, AIAA, Honolulu, HI, August 2008.

[17]Scott, M., Enke, A., and Flanagan, J., "SensorCraft Free-Flying Aeroservoelastic Model Design and Fabrication," No. 2011–1957 in AIAA Structures, Structural Dynamics and Materials Conference, AIAA, Denver, CO, April 2011.

[18]Sharma, V. and Reichenbach, E., "Development of an Innovative Support System for SensorCraft Model," No. 2011–1958 in AIAA Structures, Structural Dynamics and Materials Conference, AIAA, Denver, CO, April 2011.

[19]Reichenbach, E., Castelluccio, M., and Sexton, B., "Joined Wing Sensorcraft Aeroservoelastic Wind Tunnel Test Program," No. 2011–1956 in AIAA Structures, Structural Dynamics and Materials Conference, AIAA, Denver, CO, April 2011.

[20]Scott, R., Castelluccio, M., Coulson, D., and Heeg, J., "Aeroservoelastic Wind-Tunnel Tests of a Free-Flying, Joined-Wing Sensorcraft Model for Gust Load Alleviation," No. 2011–1960 in AIAA Structures, Structural Dynamics and Materials Conference, AIAA, Denver, CO, April 2011.

[21]Heeg, J. and Morelli, E., "Evaluation of Simultaneous Multi-Sine Excitation of the Joined Wing Sensorcraft Aeroelastic Wind Tunnel Model," No. 2011–1959 in AIAA Structures, Structural Dynamics and Materials Conference, AIAA, Denver, CO, April 2011.